

http://pubs.acs.org/journal/aelccp

# The Role of Bicarbonate-Based Electrolytes in H<sub>2</sub>O<sub>2</sub> Production through Two-Electron Water Oxidation

Thomas Mark Gill, Lauren Vallez, and Xiaolin Zheng\*



Cite This: ACS Energy Lett. 2021, 6, 2854-2862



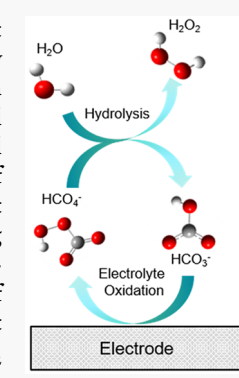
**ACCESS** 

III Metrics & More

Article Recommendations

Supporting Information

ABSTRACT: Two-electron water oxidation (2e¯WOR) is a promising route toward efficient production of a valuable product in  $H_2O_2$ . Recent attention has focused on developing new electrocatalysts for 2e¯WOR, but the role of the electrolyte species in determining water oxidation selectivity and promoting 2e¯WOR has not been established. Here, we use electroanalytical experiments to confirm the role of  $HCO_3^-$  as a selective 2e¯WOR redox catalyst. We find minimal differences in  $H_2O_2$  consumption pathways among common electrolytes, indicating that the role of  $HCO_3^-$  is to promote  $H_2O_2$  production. Mechanistically, our rotating ring disk experiments show that  $H_2O_2$  is not generated directly at the disk electrode in KHCO3 but formed after a time delay, suggesting electrolyte oxidation and subsequent hydrolysis as the promotional mechanism. Further electrochemical and spectroscopic experiments confirm this hypothesis, demonstrating anodic oxidation of carbonaceous electrolyte species occurs at Faradaic potentials relevant for water oxidation and that these species (likely  $HCO_4^-$  or  $C_2O_6^{2-}$ ) subsequently oxidize water to  $H_2O_2$  ( $t_{1/2} \approx 5$  min). The  $H_2O_2$  production rate at 2.5 V vs RHE scales linearly with the concentration of  $HCO_3^-$ , confirming the



catalytic role of HCO<sub>3</sub><sup>-</sup> in 2e<sup>-</sup>WOR and suggesting the electrolyte can be leveraged to enhance electrochemical H<sub>2</sub>O<sub>2</sub> production.

ydrogen peroxide (H<sub>2</sub>O<sub>2</sub>) exhibits strong oxidizing properties with benign byproducts, making it useful in wastewater treatment, bleaching, and chemical synthesis.<sup>3</sup> H<sub>2</sub>O<sub>2</sub> can also serve as both a fuel and oxidizer in single-compartment fuel cells, making it an emergent energy storage chemical.<sup>4-6</sup> Though H<sub>2</sub>O<sub>2</sub> is currently produced by the anthraquinone process, its electrochemical production via two-electron water oxidation (2e-WOR) has recently garnered research attention as a potential means to store renewable electricity. 7-10 Because 2e-WOR is thermodynamically less favorable than the oxygen evolution reaction (OER), substantial efforts have aimed to establish active and selective electrocatalysts for 2e-WOR. Little work has systematically studied the role of electrolytes in modulating the selectivity of WOR, despite the electrolyte species being known to greatly affect water oxidation selectivity. Sayama et al. first reported that KHCO<sub>3</sub> yields the greatest amount of H<sub>2</sub>O<sub>2</sub> among LiSO<sub>4</sub>, NaClO<sub>4</sub>, H<sub>3</sub>BO<sub>3</sub>, phosphate buffer, and K<sub>2</sub>CO<sub>3</sub> electrolytes over fluorine-doped tin oxide (FTO) surfaces. 11 The importance of HCO<sub>3</sub><sup>-</sup> in promoting H<sub>2</sub>O<sub>2</sub> formation was recognized, and HCO<sub>3</sub><sup>-</sup>-based electrolytes have since been used broadly for  $H_2O_2$  production through  $2e^-WOR$ .  $^{7-9,12-14}$ It was postulated that aqueous bicarbonate (HCO<sub>3</sub><sup>-</sup>) itself may be oxidized at the anode to peroxymonocarbonate  $(HCO_4^-)$  and/or peroxydicarbonate  $(C_2O_6^{2-})$ , which then

oxidize water to produce  $HCO_3^-$  and  $H_2O_2$ . Moreover, several other mechanisms have been suggested to explain the promotional role of  $HCO_3^-$  in  $H_2O_2$  production, including enhanced homogeneous stability of  $H_2O_2$  in bicarbonate solutions, the buffering effect of  $HCO_3^-$ , and  $HCO_3^-$  preventing further oxidation of  $H_2O_2$  at the electrode surface. Recent reviews have concluded that experimental evidence for the role of  $HCO_3^-$  is incomplete at best. 17

Here, we use a combination of electrochemical and spectroscopic methods to investigate the role of bicarbonate-based electrolyte species ( $HCO_3^-$  and  $CO_3^{2-}$ ) for  $2e^-WOR$ . We use  $BiVO_4$  as an anode throughout, as it is among the most selective electrocatalysts for  $2e^-WOR$ . First, we determine the electrochemical production rate of  $H_2O_2$  by accounting for both the accumulated  $H_2O_2$  and  $H_2O_2$  lost though homogeneous decomposition and anodic oxidation. We find  $H_2O_2$  production increases in the order of  $Na_2SO_4 < KPi < K_2CO_3 < KHCO_3$ , confirming the promotional effect of

Received: June 18, 2021 Accepted: July 19, 2021 Published: July 22, 2021





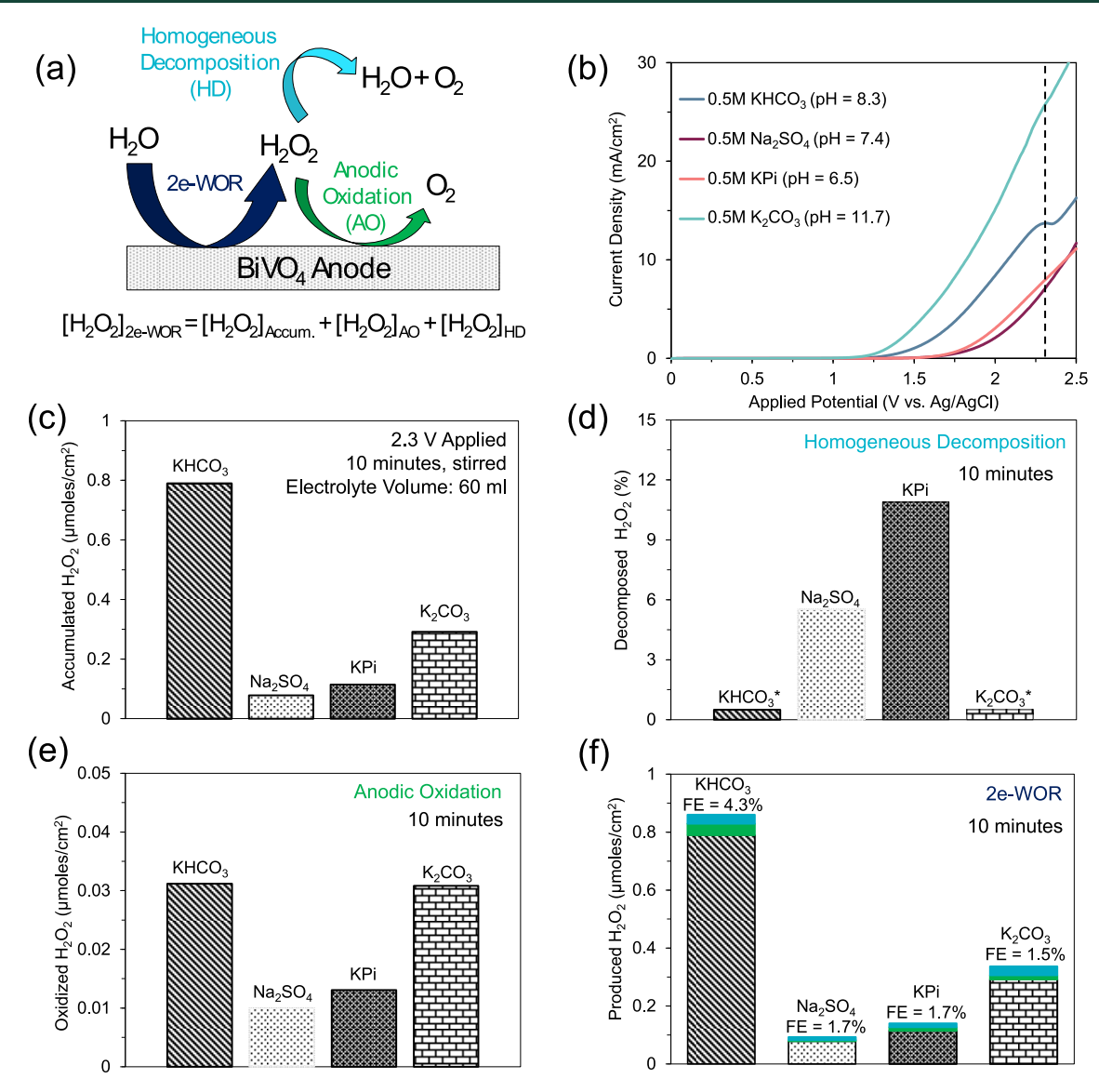


Figure 1. Accounting for production and consumption pathways of  $H_2O_2$  in various 0.5 M aqueous electrolytes. A constant potential of 2.3 V was applied between BiVO<sub>4</sub> samples and a Ag/AgCl reference electrode for 10 min in a 60 mL H-cell under vigorous stirring. All  $H_2O_2$  amounts were determined by UV—vis spectroscopy. (a) Schematic representation of pathways relevant to  $H_2O_2$  during two-electron water oxidation (2e-WOR). (b) Linear sweep voltammograms obtained in each of the four electrolytes at a scan rate of 25 mV/s. The dashed black line indicates the applied potential in subsequent tests. (c) Total  $H_2O_2$  accumulated in the anodic chamber of the H-cell. (d) Decomposition of  $H_2O_2$  due to homogeneous instability. (e) Amount of  $H_2O_2$  oxidized at the anode as determined by the peroxide addition method. (f) Total amount of  $H_2O_2$  produced by 2e-WOR after correcting for losses due to anodic oxidation (green) and homogeneous decomposition (blue) and corresponding Faradaic efficiency (FE) toward  $H_2O_2$ . \* $H_2O_2$  decomposition in KHCO<sub>3</sub> and  $K_2CO_3$  were found to be negligible over time scales of the experiment. See the Supporting Information (Figure S1b) for details.

carbonate-based electrolytes, and that KHCO<sub>3</sub> exhibits selectivity approximately 3-fold higher than that of the other electrolytes. Second, we find that less than 19% of produced H<sub>2</sub>O<sub>2</sub> is consumed by homogeneous decomposition and anodic oxidation combined under our experimental conditions (<1 h) in all electrolytes studied. Together, these results suggest that the dominant role of HCO<sub>3</sub><sup>-</sup> in 2e<sup>-</sup>WOR is neither homogeneous nor anodic stabilization of H<sub>2</sub>O<sub>2</sub> but rather generation of H<sub>2</sub>O<sub>2</sub>. Combining rotating ring disk, voltammetric, and spectroscopic experiments, we demonstrate that oxidation of carbonaceous electrolyte species occurs at Faradaic potentials for 2e<sup>-</sup>WOR, which we speculate subsequently oxidize water to H<sub>2</sub>O<sub>2</sub>. Finally, we show that the partial current density toward H<sub>2</sub>O<sub>2</sub> increases linearly with

the concentration of  $HCO_3^-$  at 2.5 V vs RHE but that this relationship changes at higher potential. Together, these findings establish that  $HCO_3^-$  serves as a redox catalyst in  $H_2O_2$  production at relatively modest potentials but that the roles of  $HCO_3^-$  and other carbonate-based species are likely potential-dependent.

To understand the role of electrolytes in  $H_2O_2$  production, the multitude of reactions in which  $H_2O_2$  can be involved under 2e<sup>-</sup>WOR conditions must be considered.  $H_2O_2$  may be produced by 2e<sup>-</sup>WOR but can be consumed by two subsequent pathways (Figure 1a). First, the thermodynamic potential for  $H_2O_2$  generation by 2e<sup>-</sup>WOR (1.76 V vs RHE) is sufficiently positive to oxidize  $H_2O_2$  to  $O_2$  (0.68 V vs RHE)<sup>19</sup> by anodic oxidation (AO). Second,  $H_2O_2$  can homogeneously

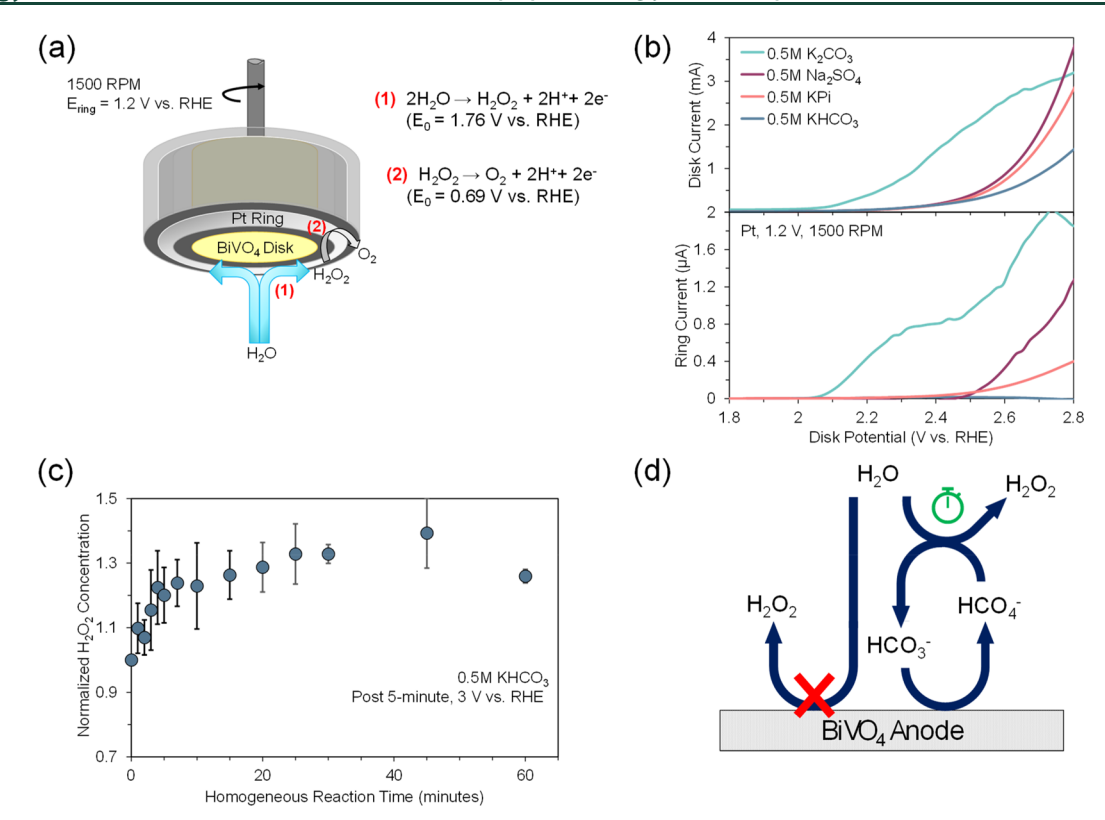


Figure 2. Hydrodynamic and equilibration experiments demonstrating the unique electrochemical oxidation behavior in KHCO<sub>3</sub>. (a) Schematic representation of rotating ring disk electrode experiment and reactions. (b) Disk and ring current during a linear sweep of the disk potential at a scan rate of 10 mV/s. (c) Normalized concentration of  $H_2O_2$  present in a single-compartment electrochemical cell after conclusion of a constant potential test. The measured  $H_2O_2$  concentration is normalized by the concentration of  $H_2O_2$  measured immediately after the conclusion of the constant potential test by colorimetric strips. Error bars indicate sample standard deviation. (d) Schematic representation of the reaction mechanism in which  $HCO_3^-$  is electrochemically oxidized, followed by hydrolysis to produce  $H_2O_2$ .

decompose (HD) to  $H_2O$  and  $O_2$  in aqueous solutions, especially in the presence of ions that catalyze  $H_2O_2$  decomposition. In previous studies, the accumulated amount of  $H_2O_2$  has been used almost universally to characterize the Faradaic efficiency (FE) of  $2e^-WOR$ . However, this method accounts only for the net difference between the production of  $H_2O_2$  and its consumption through AO and HD. It is necessary to evaluate the effect of the electrolyte species on each of these pathways to understand the role of bicarbonate in maximizing  $2e^-WOR$  efficiency.

We investigate the impact of the electrolyte in 2e WOR by quantifying the production and consumption of H<sub>2</sub>O<sub>2</sub> (reaction fluxes) in four common electrolyte species: sodium sulfate (Na<sub>2</sub>SO<sub>4</sub>), potassium phosphate buffer (KPi), potassium carbonate (K<sub>2</sub>CO<sub>3</sub>), and potassium bicarbonate (KHCO<sub>3</sub>) all at 0.5 M concentration (for details, see Figure S1 and supplementary note 1 in the Supporting Information). For all tests, we use sol-gel derived bismuth vanadate thin films (BiVO<sub>4</sub>; thickness, ~100 nm; area range, 3-4 cm<sup>2</sup>) coated on FTO substrates as the anode. 12 Figure 1b shows that the four electrolytes exhibit distinct current densities at the same applied potential. We compare the H<sub>2</sub>O<sub>2</sub> reaction fluxes at 2.3 V vs Ag/AgCl at which the current density (>5 mA/ cm<sup>2</sup>) is large enough for appreciable H<sub>2</sub>O<sub>2</sub> accumulation on short time scales in all electrolytes studied. Panels c, d, e and f in Figure 1 show the experimentally determined H<sub>2</sub>O<sub>2</sub> fluxes for accumulation, HD, AO, and calculated H<sub>2</sub>O<sub>2</sub> production by 2e-WOR after 10 min of reaction, respectively. Figure 1c shows that KHCO<sub>3</sub> yields the highest accumulated H<sub>2</sub>O<sub>2</sub>

amount of 0.8  $\mu$ mol/cm<sup>2</sup>, while K<sub>2</sub>CO<sub>3</sub> is second with 0.3 μmol/cm<sup>2</sup>, more than 2.5 times that of KPi and Na<sub>2</sub>SO<sub>4</sub>. Though the superiority of K<sub>2</sub>CO<sub>3</sub> over other electrolytes is small, Li and co-workers recently reported similar results on H<sub>2</sub>O<sub>2</sub> production rates among KHCO<sub>3</sub>, K<sub>2</sub>CO<sub>3</sub>, and KH<sub>2</sub>PO<sub>4</sub>/ K<sub>2</sub>HPO<sub>4</sub> at 1 M concentrations evaluated at 2.8 V vs RHE, confirming the promotional effect of carbonaceous species.<sup>21</sup> Though the promotional effect of HCO3- was shown, no explicit investigation was made as to the role it plays in H<sub>2</sub>O<sub>2</sub> production, consumption, and stabilization. Figure 1d shows that H<sub>2</sub>O<sub>2</sub> loss through HD over 10 min is negligible for KHCO<sub>3</sub> and K<sub>2</sub>CO<sub>3</sub> but significant for both KPi (~11%) and  $Na_2SO_4$  (~6%). The amount of  $H_2O_2$  consumed by anodic oxidation (Figure 1e) is most substantial in the K<sub>2</sub>CO<sub>3</sub> and KHCO<sub>3</sub> electrolytes ( $\sim 0.03 \, \mu \text{mol/cm}^2$ ), corresponding to the destruction of  $\sim$ 11% and  $\sim$ 4% of the accumulated  $H_2O_2$ , respectively. Note that the magnitude of AO is expected to depend strongly on the electrocatalyst surface. For example, the normalized AO current on our BiVO4 electrode is estimated to be  $\sim 11 \,\mu\text{A/cm}^2 \cdot \text{mM H}_2\text{O}_2$ , more than an order of magnitude smaller than the AO current on Pt in phosphate buffer at comparable mixing speed (~600 μA/cm<sup>2</sup>·mM H<sub>2</sub>O<sub>2</sub>).<sup>22</sup> The total amount of H<sub>2</sub>O<sub>2</sub> produced by 2e<sup>-</sup>WOR calculated using eq 1 (Figure 1f) decreases in the order of  $KHCO_3 > K_2CO_3 > KPi > Na_2SO_4$ , which matches the trend using accumulated H<sub>2</sub>O<sub>2</sub> (Figure 1c).

$$[H_2O_2]_{2e\text{-WOR}} = [H_2O_2]_{Accum.} + [H_2O_2]_{AO} + [H_2O_2]_{HD}$$
(1)

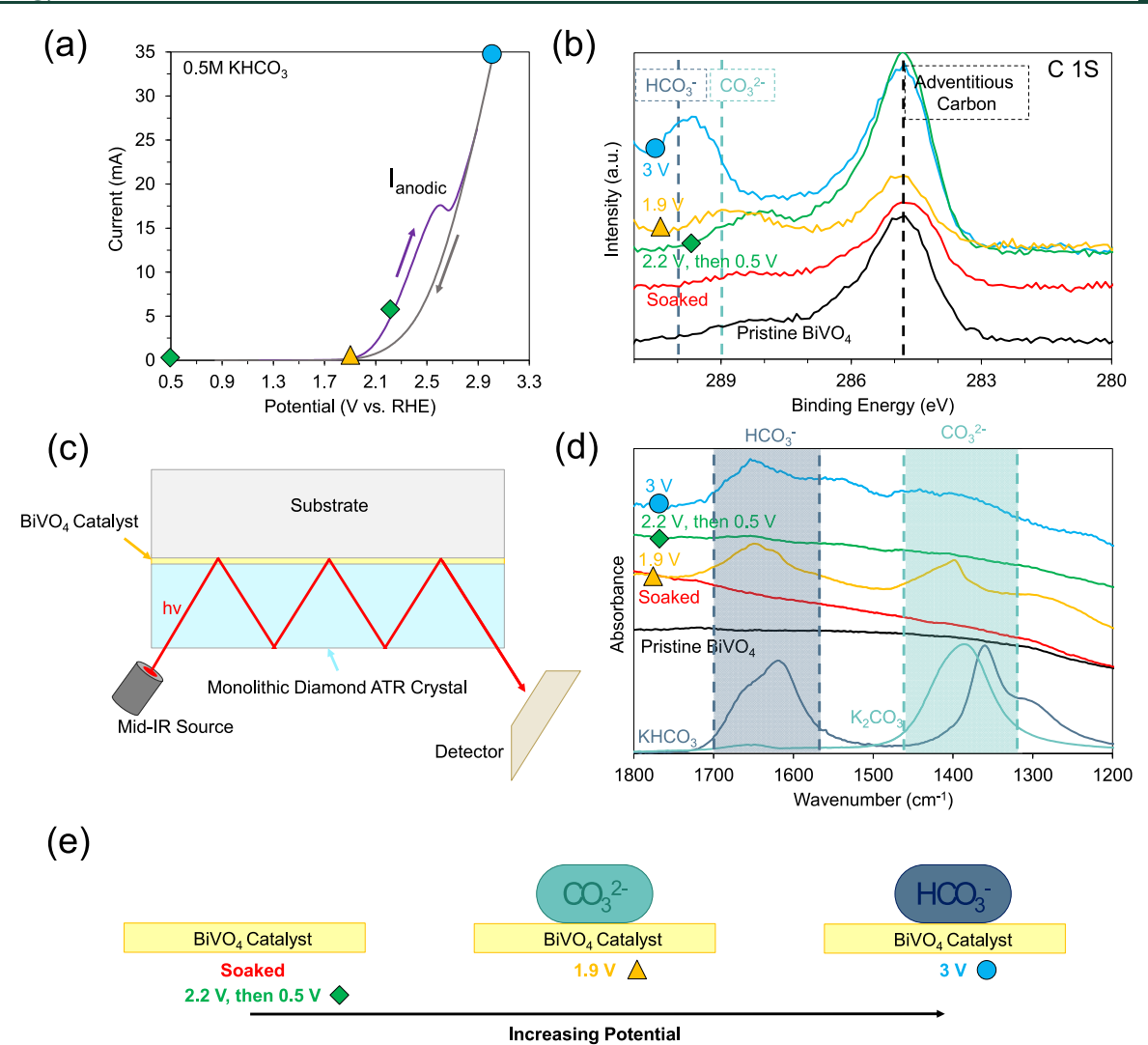


Figure 3. Spectroscopic and electrochemical evidence for oxidation of the electrolyte and its subsequent interaction with the electrode surface. (a) Characteristic cyclic voltammogram obtained at 250 mV/s in 0.5 M KHCO<sub>3</sub> showing a prominent peak feature in the anodic sweep. Arrows indicate sweep direction, and marker shapes and colors correspond to spectroscopic traces in panels b and d indicating potentials applied therein. (b) X-ray photoelectron spectra taken after subjecting the samples to the indicated bias for 10 min in 0.5 M KHCO<sub>3</sub>, followed by cleaning in water. (c) Schematic of ATR-FTIR experimental setup. (d) Fourier transform infrared spectra for the same samples depicted in panel b along with solution-phase spectra of 0.5 M KHCO<sub>3</sub> and K<sub>2</sub>CO<sub>3</sub> for reference. (e) Schematic representation of surface-adsorbed species as a function of applied potential.

Accordingly, the use of accumulated  $\rm H_2O_2$  is a reasonable approximation to estimate FE under our experimental conditions, but this approximation underestimates FE significantly (18% (relative) in KPi for 10 min). The FE in KHCO<sub>3</sub> (~4.3%) is nearly 3 times higher than the other three electrolytes (~1.6%), confirming the previously observed superior performance of KHCO<sub>3</sub> (more generally HCO<sub>3</sub><sup>-</sup>) and to a lesser extent  $\rm CO_3^{2-,10}$  for electrochemical production of  $\rm H_2O_2^{11}$  These results demonstrate the importance of considering all relevant reaction fluxes in future  $\rm 2e^-WOR$  studies. We emphasize that the metrics for  $\rm H_2O_2$  production and consumption found here likely depend on the electrochemical cell setup and test duration (see supplementary note 2 in the Supporting Information for further discussion).

The above reaction flux analysis reveals the complexity in understanding 2e<sup>-</sup>WOR performance by measuring accumulated H<sub>2</sub>O<sub>2</sub> due to its instability in electrochemical environments. In comparison, H<sub>2</sub>O<sub>2</sub> produced by 2e<sup>-</sup>WOR can be directly quantified by rotating ring disk electrode (RRDE)

measurements. In these experiments, H<sub>2</sub>O<sub>2</sub> is produced on the BiVO<sub>4</sub> disk electrode and subsequently oxidized to O<sub>2</sub> on the platinum (Pt) ring electrode held at 1.2 V vs RHE (Figure 2a). Because the RRDE assembly is rotated at 1500 rpm, little time transpires between production and measurement, minimizing the consumption of H<sub>2</sub>O<sub>2</sub> by anodic oxidation and homogeneous decomposition. Moreover, at 1.2 V vs RHE, the only substantial reaction at the ring is the oxidation of H<sub>2</sub>O<sub>2</sub> to O<sub>2</sub> (Figure S2). Figure 2b shows the disk and ring currents versus disk potential for the four electrolytes, their resulting ratio being proportional to the FE toward H<sub>2</sub>O<sub>2</sub> under mass transport limited conditions. 23,24 Unfortunately, the evolution of O2 gas at the ring and disk electrodes at higher electric potentials (>2.8 V vs RHE) yields very noisy data, preventing exact FE quantification and direct comparison with accumulation-based data in Figure 1f. Still, the ring current in each electrolyte excluding KHCO3 has an onset potential similar to that of the disk current, indicating that some of the oxidative current at the disk is attributable to direct 2e-WOR.

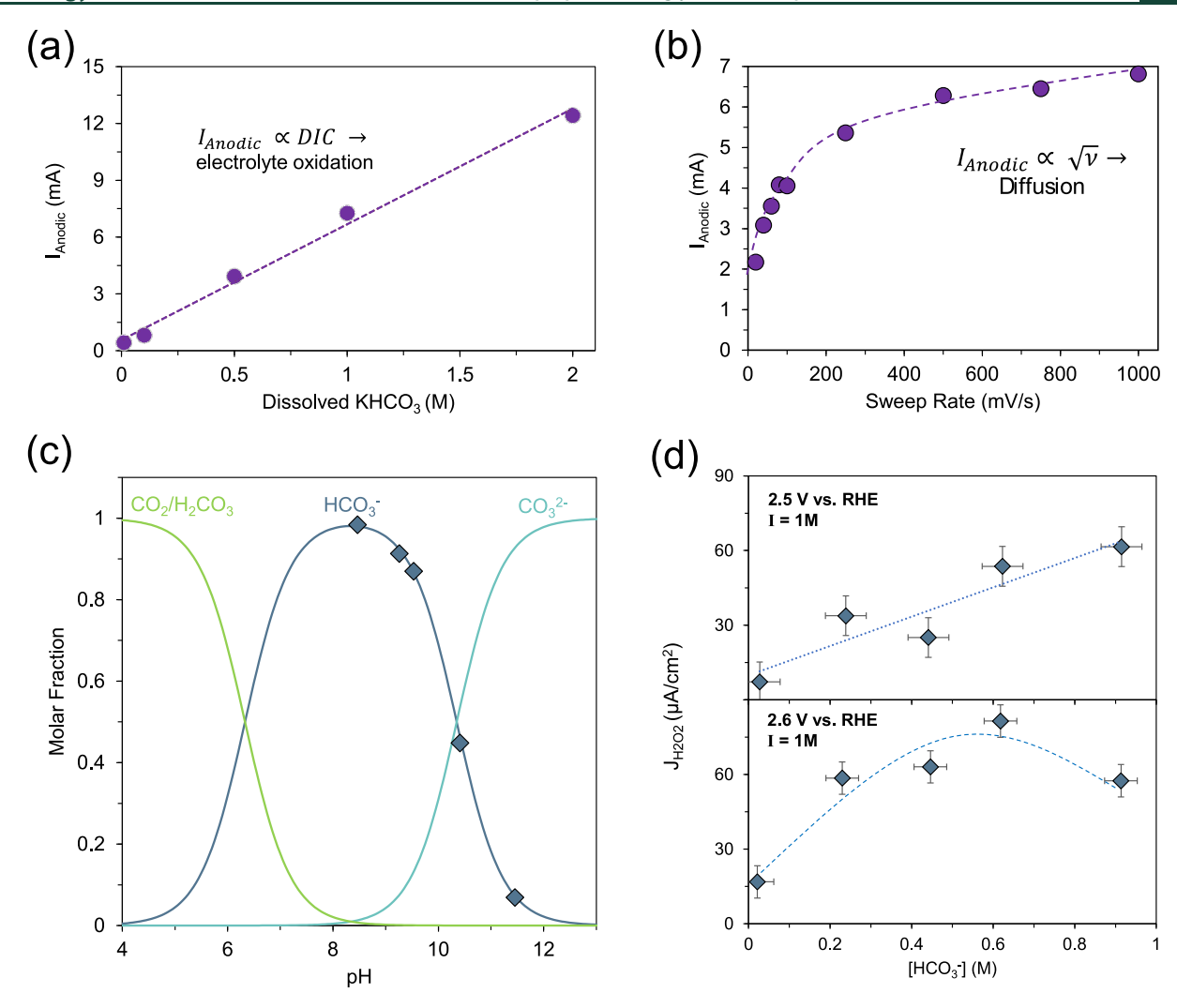


Figure 4. Relation between bulk concentrations of electrolyte species, overall current, and  $H_2O_2$  partial current density. (a) Linear relationship between dissolved KHCO<sub>3</sub> concentration (alternatively, dissolved inorganic carbon, "DIC") and the anodic peak current,  $I_{\text{anodic}}$  obtained under constant ionic strength conditions (I = 2 M) with KClO<sub>4</sub> as a supporting electrolyte. (b) Square root dependence of  $I_{\text{anodic}}$  on the scan rate indicating a diffusion-limited current.  $I_{\text{anodic}}$  was determined by subtracting the cathodic from the anodic current at the peak potential. Dashed lines are guides-to-the-eye, not fits to the data. (c) Equilibrium mole fractions of dissolved inorganic carbon species as a function of pH, known as a Bjerrum plot, calculated using the first and second acid dissociation constants of carbonic acid (3.6 and 10.3, respectively). Diamonds indicate pH/molar fractions tested in panel d. (d) Partial current density toward  $H_2O_2$  as a function of HCO<sub>3</sub><sup>-</sup> concentration. The ionic strength was held constant (I = 1 M), and the indicated bias was applied for 10 min in an H-cell under vigorous stirring. Vertical error bars indicate measurement uncertainty. Horizontal error bars indicate concentration error due to variation in the bulk solution pH. Dashed lines are guides-to-the-eye, not fits to the data.

However, there is no measurable ring current for KHCO<sub>3</sub> even as its disk current rises appreciably. This suggests that a negligible amount of H<sub>2</sub>O<sub>2</sub> is directly produced on the BiVO<sub>4</sub> disk in 0.5 M KHCO3, seemingly contradicting the enhanced production of H<sub>2</sub>O<sub>2</sub> in KHCO<sub>3</sub> shown in Figure 1f. One possible explanation for the discrepancy is that H2O2 is not primarily produced by direct 2e<sup>-</sup>WOR on the BiVO<sub>4</sub> anode in KHCO<sub>3</sub>, but by other reactions which may include oxidation of the electrolyte. 11,25 In contrast to these results, Zhang and co-workers recently observed a measurable H2O2 ring current in 1 M NaHCO<sub>3</sub> stemming from a BiVO<sub>4</sub> disk electrode.<sup>26</sup> Given the differing ring electrode material (BiVO<sub>4</sub>), electrolyte cation (Na<sup>+</sup>), disk potential (<2.25 V vs RHE), and electrolyte concentration (1 M), substantial differences between their RRDE results and ours are expected. Despite these differences, Zhang's work and ours yield similar qualitative conclusions about the direct water oxidation pathway: given the ratio of ring ( $\sim$ 5  $\mu$ A) to disk ( $\sim$ 500  $\mu$ A) currents observed in their study, direct water oxidation to H<sub>2</sub>O<sub>2</sub> on BiVO<sub>4</sub> is a relatively minor pathway in HCO<sub>3</sub><sup>-</sup> electrolytes. Further discussion is offered in the Supporting Information (supplementary note 3).

For KHCO<sub>3</sub> electrolytes, we test the possibility of  $H_2O_2$  produced homogeneously via oxidation of the electrolyte by measuring the  $H_2O_2$  concentration as a function of time after applying a potential to the anode. We applied 3 V vs RHE to  $BiVO_4$  for 5 min in a single-compartment electrochemical cell to accumulate a measurable amount of  $H_2O_2$  and then stopped the bias. If  $H_2O_2$  is produced by a homogeneous reaction between the oxidized electrolyte and water, the concentration of  $H_2O_2$  should increase over time, which is indeed revealed by the data (Figure 2c). This anomalous increase in  $H_2O_2$  was also observed during the homogeneous decomposition experiments (Figure S1b). The concentration of  $H_2O_2$  takes ~15–20 min to equilibrate, a time scale similar to the previously

reported kinetics for the reaction between  $HCO_4^-$  and  $H_2O$  to form  $H_2O_2$  ( $t_{1/2}\approx 5$  min). Because of this minutes-long time scale, the observed near-zero ring current for KHCO3 in the RRDE experiments is presumably due to insufficient time for the homogeneous following reaction to produce  $H_2O_2$  during the transit from the disk to the ring (Figure 2b). These results support the hypothesis suggested by Sayama that  $HCO_3^-$  is electrochemically oxidized, followed by hydrolysis to yield  $H_2O_2$  (Figure 2d). We will refer to the oxidized electrolyte species as  $HCO_4^-$ , though several attempts to identify the exact species were unsuccessful. Patra et al. And Zhang and Oloman have provided a more detailed mechanistic description of carbonate and bicarbonate oxidation, which has been adapted and summarized in supplementary note 4 in the Supporting Information.

If HCO<sub>3</sub> is electrochemically oxidized at the anode, spectroscopic signatures of the species may be visible when studying the anode surface. We used electroanalytical and spectroscopic experiments to investigate surface-bound carbonaceous species resulting from the KHCO3 electrolyte. Figure 3a shows a typical cyclic voltammogram (CV) of the BiVO<sub>4</sub> anode in 0.5 M KHCO3. One observable feature, an anodic peak (the current at which is denoted  $I_{anodic}$ ), motivated us to use X-ray photoelectron spectroscopy (XPS) and attenuated total reflection Fourier transform infrared spectroscopy (FTIR) to determine the surface-bound species on BiVO<sub>4</sub> at different applied potentials relative to the feature. We characterized five BiVO<sub>4</sub> samples: pristine, submerged in KHCO<sub>3</sub> without applying potential (soaked), subjected to 1.9 V, subjected to 3.0 V, and one sample first subjected to an oxidizing potential (2.2. V) and then a more cathodic potential (0.5 V). All indicated potentials are voltages versus a reversible hydrogen electrode (RHE) and were held for 10 min. The four BiVO<sub>4</sub> samples that contacted the electrolyte were thoroughly rinsed and sonicated in deionized water for 1 min followed by drying with air to remove residual electrolyte. The carbon 1s region was probed using XPS to study surface-bound carbonaceous species because of its surface sensitivity. Here, the peak at ~290 eV indicates HCO<sub>3</sub><sup>-</sup> and ~289 eV indicates CO3<sup>2-;29</sup> 284.8 eV indicates the adventitious carbon used for calibrating the data (Figure 3b). For FTIR measurements samples were placed on a diamond ATR crystal with the BiVO<sub>4</sub> catalyst facing the crystal to achieve greater surface sensitivity through multiple internal reflections (Figure 3c). KHCO<sub>3</sub> and K<sub>2</sub>CO<sub>3</sub> solutions were measured as references to identify the wavelength range for HCO<sub>3</sub><sup>-</sup> (1550-1700 cm<sup>-1</sup>) and CO<sub>3</sub><sup>2-</sup> (1320–1450 cm<sup>-1</sup>) derived species.<sup>30</sup>

The XPS and FTIR spectra (Figure 3b,d) reveal similar information. First, neither pristine nor soaked BiVO<sub>4</sub> samples exhibit any signatures of HCO<sub>3</sub><sup>-</sup> and CO<sub>3</sub><sup>2</sup><sup>-</sup>. Second, the BiVO<sub>4</sub> samples that have been exposed to high (1.9 and 3.0 V) potential show the presence of CO<sub>3</sub><sup>2</sup><sup>-</sup> and HCO<sub>3</sub><sup>-</sup>, respectively. The 1.9 V sample more prominently shows surface-bound CO<sub>3</sub><sup>2</sup><sup>-</sup>, while 3.0 V shows surface-bound HCO<sub>3</sub><sup>-</sup> based on the XPS spectra. Moreover, the 3.0 V sample shows an FTIR absorption peak near 1650 cm<sup>-1</sup>, which matches relatively well with the suggested absorption of HCO<sub>4</sub><sup>-</sup> at wavenumbers of 1630 or 1685 cm<sup>-1,31</sup> Interestingly, the "2.2 V then 0.5 V" BiVO<sub>4</sub> sample shows no signs of surface-bound HCO<sub>3</sub><sup>-</sup> or CO<sub>3</sub><sup>2-</sup>. Collectively, these results indicate that CO<sub>3</sub><sup>2-</sup> and/or HCO<sub>3</sub><sup>-</sup> are present on the BiVO<sub>4</sub> anode surface at potentials necessary to generate H<sub>2</sub>O<sub>2</sub> but may not be present at lower bias or under potential cycling. Moreover,

 $HCO_3^-$  seems to predominate at higher anodic potential, whereas modest Faradaic bias favors  $CO_3^{2-}$  (Figure 3e). The presence of  $CO_3^{2-}$  on the surface despite the near-neutral pH in the bulk electrolyte ( $\sim$ 8) may be explained by the dramatically different surface and bulk equilibria observed in bicarbonate systems, especially at elevated potentials. In conjunction with the greater production of  $H_2O_2$  observed in the bicarbonate-based electrolytes, it is apparent that these surface-bound species are involved in the production of  $H_2O_2$ , though further spectroscopic studies are needed to fully understand their mechanistic role. In particular, Raman spectroscopy has recently shown potential as a technique for observing  $HCO_3^-$  and its derivatives on electrochemical surfaces. Signature of the production of the p

Given their presence on the electrode surface during 2e-WOR and their hypothesized oxidation, the concentration of HCO<sub>3</sub><sup>-</sup> and CO<sub>3</sub><sup>2-</sup> should impact the anodic current. To study this, we varied the concentration of dissolved KHCO<sub>2</sub> in the electrolyte while keeping the ionic strength constant at 2 M using KClO<sub>4</sub> as a coelectrolyte. The previously mentioned I<sub>anodic</sub> feature shows a linear dependence on dissolved KHCO<sub>3</sub> (Figure 4a). The observed linear dependence of  $I_{\text{anodic}}$  holds while varying the ionic strength (10 mM to 2 M) as well (Figure S3a). Moreover, when the KHCO<sub>3</sub> concentration was held constant at 0.5 M, I<sub>anodic</sub> scales with the square root of scan rate  $(\nu)$  at modest scan rates, indicating a diffusionlimited process per the Randles-Sevcik equation (Figure 4b).<sup>34</sup> Stirring the electrolyte increased the current near the I<sub>anodic</sub> feature, further confirming transport-limited electrolyte oxidation (Figure S3b). These results suggest that anodic oxidation of HCO<sub>3</sub><sup>-</sup> to HCO<sub>4</sub><sup>-</sup> (1.8 V vs RHE) occurs on BiVO<sub>4</sub>. <sup>27,35</sup> Nonetheless, we cannot rule out the possibility of anodic oxidation of CO<sub>3</sub><sup>2-</sup> to carbonate radical and/or C<sub>2</sub>O<sub>6</sub><sup>2-</sup> (1.57 Vvs RHE)<sup>25</sup> as HCO<sub>3</sub><sup>-</sup> and CO<sub>3</sub><sup>2-</sup> always coexist in solution because of equilibrium.<sup>28</sup> Notably, a similar  $I_{anodic}$ feature has been observed previously on Fe-derived surfaces in acidified 0.5 M Na<sub>2</sub>CO<sub>3</sub>(pH 9.1),<sup>36</sup> and carbonate oxidation in aqueous Na<sub>2</sub>CO<sub>3</sub> on Pt has previously been demonstrated.<sup>25</sup> Though the oxidized species is uncertain, electrochemical oxidation of bicarbonate-based electrolytes clearly occurs on many surfaces and likely contributes mechanistically to 2e-WOR. Previous reports in molecular catalysis have hypothesized a similar system for H<sub>2</sub>O<sub>2</sub> production from H<sub>2</sub>O and HCO<sub>3</sub><sup>-.37</sup> Briefly, HCO<sub>4</sub><sup>-</sup> is formed as a bound intermediate on an aluminum porphyrin molecular catalyst (AlTMPyP) and is subsequently liberated by reaction with H<sub>2</sub>O to form HCO<sub>3</sub><sup>-</sup> and H<sub>2</sub>O<sub>2</sub>. Interestingly, the authors find that  $CO_3^{2-}$  can undergo a similar mechanism.

As both oxidized bicarbonate (i.e.,  $HCO_4^-$ ) and carbonate (i.e.,  $C_2O_6^{2-}$ ) can reportedly react with  $H_2O$  to produce  $H_2O_2$ ,  $^{16,25}$  we measured the current density toward  $H_2O_2$  ( $J_{H_2O_2}$ , a metric of the electrochemical production rate) as a function of  $HCO_3^-$  and  $CO_3^{2-}$  concentrations as determined by the Bjerrum plot in Figure 4c. We fixed the ionic strength at 1 M and varied the concentration of  $HCO_3^-$  by adding different ratios of  $K_2CO_3$  and  $KHCO_3$  powder to the solution. The electrochemically active surface area was determined by cyclic voltammetry and used for the normalization of the current (Figure S4a). At 2.5 V vs RHE (~740 mV overpotential for  $2e^-WOR$ ),  $J_{H_2O_2}$  increases linearly with  $[HCO_3^-]$  within error, indicating that  $HCO_3^-$  is the reactant primarily responsible for  $H_2O_2$  production (Figure 4d). At 2.6

V vs RHE, which roughly corresponds with  $I_{\text{anodic}}$  in these experiments,  $J_{H,O_2}$  first increases and then decreases or plateaus with [HCO<sub>3</sub><sup>-</sup>]. Recent work by Mavrikis et al. demonstrated that a 1:1 mixture of KHCO<sub>3</sub> and K<sub>2</sub>CO<sub>3</sub> outperforms pure KHCO3 for H2O2 production at potentials above 2.6 V vs RHE, confirming that the presence of CO<sub>3</sub><sup>2-</sup> can be beneficial for H<sub>2</sub>O<sub>2</sub> production.<sup>38</sup> This suggests that, as the electrolyte oxidation reaction becomes diffusion limited at higher bias, other competing reactions become appreciable at the anode as well.<sup>36</sup> To clarify these results, it is important to evaluate the role of the pH. As we vary the concentration of HCO<sub>3</sub><sup>-</sup>, the pH value varies from ~8.4 to ~11.5. To isolate the impact of pH, we also measured  $J_{H_2O_3}$  at constant [HCO<sub>3</sub><sup>-</sup>] but differing pH values, demonstrating that  $J_{H_2O_2}$  is agnostic to pH within error (Figure S4b). Finally, we evaluated the stability of H<sub>2</sub>O<sub>2</sub> in 0.5 M KHCO<sub>3</sub> at various pH  $(8.0 \le pH \le 12)$ , demonstrating that pH has a negligible impact over the time scale of our experiments (Figure S4c). Still, experimental results in Figures 2c, S1b, and S4c suggest that H<sub>2</sub>O<sub>2</sub> is mildly unstable in KHCO<sub>3</sub> solutions over longer time scales (>1 h), which may be addressed in future work via the use of stabilizers or sequestration. Together, these results show that the pH value has a negligible effect on H<sub>2</sub>O<sub>2</sub> production within our experimental range and further confirm the dominant role that HCO<sub>3</sub> plays in 2e WOR at modest bias.

Our experimental results demonstrate that HCO<sub>3</sub><sup>-</sup> acts as a catalyst in H<sub>2</sub>O<sub>2</sub> production through 2e<sup>-</sup>WOR processes. By independently evaluating the role that electrolytes play in H<sub>2</sub>O<sub>2</sub> generation and consumption pathways, we attribute the enhanced H<sub>2</sub>O<sub>2</sub> production observed in KHCO<sub>3</sub> to its role in the production mechanism. Principally, our electrochemical and spectroscopic experiments demonstrate that oxidation of carbonaceous electrolyte species occurs at Faradaic potentials relevant for 2e-WOR, and these species subsequently oxidize water to H<sub>2</sub>O<sub>2</sub>. In summary, HCO<sub>3</sub><sup>-</sup>/HCO<sub>4</sub><sup>-</sup> serves as a redox catalyst for H<sub>2</sub>O<sub>2</sub> production in KHCO<sub>3</sub> electrolytes, which leads to a much higher production rate of H2O2 than other tested electrolytes (i.e., Na<sub>2</sub>SO<sub>4</sub>, KPi, and K<sub>2</sub>CO<sub>3</sub>). Given the potential dependence of the relationship between  $J_{H,O}$ , and  $HCO_3^-$  and the spectroscopic results, the role of  $CO_3^{\ 2^-}$  in  $H_2O_2$  production remains uncertain. <sup>28</sup> Our results suggest complex relationships between the bulk equilibrium and surface-mediating roles  $HCO_3^-$  and  $CO_3^{2-}$  play in 2e<sup>-</sup>WOR which have been observed in other studies. <sup>28,32</sup> Furthermore, this work demonstrates the importance of evaluating reaction fluxes in 2e-WOR studies and the potential to utilize electrolyte oxidation at the anode to improve  $H_2O_2$  production rates. Operando spectroscopic studies of single-crystalline electrode surfaces, computational chemistry calculations, and detailed electrokinetic analyses are urgently desired to further specify the roles of carbonaceous anions, especially CO<sub>3</sub><sup>2-</sup>, in water oxidation.

### EXPERIMENTAL METHODS

All reagents used in this study were obtained from Sigma-Aldrich and used as received, unless otherwise noted.

Electrochemical  $H_2O_2$  Production Accounting. Production of  $H_2O_2$  was measured under chronoamperometric conditions in a glass H-cell (Pine Research). The anodic and cathodic chambers were separated by a porous frit to prevent cathodic effects from impacting  $H_2O_2$  production and

consumption. All glassware was cleaned in dilute piranha solution before use. Carbon paper was used as a counter electrode, and Ag/AgCl as a reference. All electrochemical experiments were carried out using a Gamry Interface 1000 or 1010 potentiostat. For the accumulation-based  $\rm H_2O_2$  experiments detailed in Figure 1, studies were conducted at 2.3 V applied electric potential sustained for 10 min under constant vigorous stirring of the anodic chamber of an H-cell to prevent concentration polarization.

**Electrode Preparation.** For accumulation experiments, monoclinic scheelite bismuth vanadate (BiVO<sub>4</sub>) was synthesized on fluorine-doped tin oxide (FTO) substrates as previously described. Briefly, bismuth nitrate pentahydrate (Bi(NO<sub>3</sub>)<sub>3</sub>·5H<sub>2</sub>O, >98%) and vanadyl acetylacetonate ( $C_{10}H_{14}O_5V$ , >98%) were dissolved in a solvent mixture of 2-methoxyethanol, glacial acetic acid, and acetylacetone. The resulting precursor solution was then spin-coated on the FTO substrate, followed by annealing in air at 500 °C.

 $H_2O_2$  Measurement Procedure. For all  $H_2O_2$  quantifications excluding those in Figure 2c (which used Quantofix colorimetric strips for  $H_2O_2$  detection), the previously established cobalt/carbonate UV—vis procedure was utilized. Briefly, an aliquot of the electrochemically produced  $H_2O_2$  (0.5–2.0 mL) was added to a 2 M solution of KHCO<sub>3</sub> and CoSO<sub>4</sub>. The solution was allowed to react for 30 min, after which the absorbance at 260 nm was measured. Calibrations were obtained independently in each electrolyte and were recreated each day. All spectra were collected using an Agilent Cary 6000i spectrophotometer at 1 nm resolution and a scan rate of 2 nm/s and baseline corrected using the background matrix containing no  $H_2O_2$ .

Rotating Ring Disk Electrode Experiments. Rotating ring disk electrode (RRDE) experiments were carried out using a Pine Research setup with the rotation rate controlled by a Gamry RDE710 modulator. All experiments were carried out in a glass heart cell using an E6R1PK tip assembly with a platinum ring electrode and a glassy carbon disk insert.

For the preparation of the BiVO<sub>4</sub> disk electrode in the RRDE experiments, a novel precipitation procedure was used. The same precursor as was used for the spin-coating method was first prepared. The precursor solution was then placed in an oil bath at 100 °C and was magnetically stirred, resulting in a color change of the precursor solution to transparent brown, followed by an opaque reddish color after about 10 min. A 250 uL portion of commercial hydrogen peroxide solution was then added (H<sub>2</sub>O<sub>2</sub>, 30 wt %, Fisher Chemical), followed by 50 mL of deionized water. The solution was allowed to settle, and the supernatant liquid was decanted. The successive additions of H<sub>2</sub>O<sub>2</sub> and water were repeated, ultimately resulting in a bright yellow precipitate indicative of BiVO<sub>4</sub> powder. The supernatant was again decanted, after which the powder was collected by filtration, followed by drying on a hot plate at 100 °C for 3 h to remove any residual solvent. Finally, the dry powder was annealed in a box furnace at 500 °C to allow for crystallization, and the resulting monoclinic scheelite phase was confirmed by X-ray diffraction.

The BiVO<sub>4</sub> powder was then prepared in a catalyst ink by adding 2 mg of the powder to 2 mL of isopropyl alcohol, 600  $\mu \rm L$  of deionized water, and 320  $\mu \rm L$  of Nafion (Fuel Cell Earth). The catalyst ink was sonicated for 30 min to ensure homogeneous dispersion and was subsequently drop cast on the glassy carbon insert, followed by drying in a box furnace at 160 °C for 10 min.

**Spectroscopic Experiments.** X-ray photoelectron spectra were collected using a PHI VersaProbe 3. Radiation was supplied with an Al ( $K\alpha$ ) source (1486 eV) at a vacuum pressure of  $\sim 1.2 \times 10^{-7}$  Pa and a spot size of 1400  $\mu$ m  $\times$  100  $\mu$ m under the "high power setting" to improve the signal-tonoise ratio.

Attenuated total reflectance Fourier transform infrared spectroscopy (ATR-FTIR) was conducted using a Nicolet iS-50 FTIR spectrometer and a monolithic diamond ATR element. Results, as shown, are the average of 64 scans which are background subtracted using air as a standard.

 $HCO_3^-$  Impact on  $J_{H_2O_2}$ . Experiments relating the concentration of HCO<sub>3</sub><sup>-</sup> to the current density toward H<sub>2</sub>O<sub>2</sub> were conducted chronoamperometrically at the indicated electric potential in an electrochemical H-cell with a porous glass frit separating the anodic and cathodic chambers. Notably, we elected to perform these experiments under the constant overpotential condition on an RHE scale. The electrolyte was vigorously stirred using a magnetic stir bar. The pH was measured using a Mettler Toledo FiveEasy plus probe. Because of the observed increase of the H2O2 concentration over time, H2O2 was measured using the aforementioned UV-vis procedure after allowing for 15 min of equilibration, post chronoamperometry. The electrochemically active surface area used for current density normalization was found using cyclic voltammetry in a non-Faradaic region of the voltammogram and varying the sweep rate from 250 to 1000 mV/s.

#### ASSOCIATED CONTENT

# Supporting Information

The Supporting Information is available free of charge at https://pubs.acs.org/doi/10.1021/acsenergylett.1c01264.

Detailed experimental schematics, procedures for quantifying anodic oxidation of  $H_2O_2$ , rotating ring disk control experiments, supplementary voltametric evidence for electrolyte oxidation, electrochemically active surface area quantification, impact of pH on  $H_2O_2$  stability, detailed mechanistic description of electrolyte oxidation leading to  $H_2O_2$  production, and supplementary notes which provide further context for experimental findings (PDF)

### AUTHOR INFORMATION

# **Corresponding Author**

Xiaolin Zheng — Department of Mechanical Engineering, Stanford University, Stanford, California 94305, United States; orcid.org/0000-0002-8889-7873; Email: xlzheng@stanford.edu

## Authors

Thomas Mark Gill — Department of Mechanical Engineering, Stanford University, Stanford, California 94305, United States; o orcid.org/0000-0002-0108-1012

Lauren Vallez – Department of Mechanical Engineering, Stanford University, Stanford, California 94305, United States

Complete contact information is available at: https://pubs.acs.org/10.1021/acsenergylett.1c01264

#### **Author Contributions**

T.M.G. and X.L.Z. conceived of the overall study and the design of experiments. T.M.G. conducted all experiments excluding XPS spectra, which were obtained by L.V. T.M.G. and X.L.Z. wrote the manuscript.

#### Notes

The authors declare no competing financial interest.

#### ACKNOWLEDGMENTS

X.L.Z. would like to thank the National Science Foundation EFRI-DcheM program (Agreement Number: SUB0000425), Stanford Natural Gas Initiative, Stanford Woods Institute for the Environment for their generous support. T.M.G. thanks the National Science Foundation for their support through the Graduate Research Fellowship Program and Stanford University for their support through the Stanford Graduate Fellowship in Science and Engineering. Part of this work was performed at the Stanford Nano Shared Facilities (SNSF), supported by the National Science Foundation under Award ECCS-2026822.

#### REFERENCES

- (1) Xu, J.; et al. Organic wastewater treatment by a single-atom catalyst and electrolytically produced  $H_2O_2$ . Nat. Sustain. 2021, 4, 233–241.
- (2) Wu, Y.; Wu, J.; Yang, F.; Tang, C.; Huang, Q. Effect of H<sub>2</sub>O<sub>2</sub> Bleaching Treatment on the Properties of Finished Transparent Wood. *Polymers (Basel, Switz.)* **2019**, *11*, 776.
- (3) Kang, F.; Leng, Y.; Zhang, T. Y. Influences of H<sub>2</sub>O<sub>2</sub> on synthesis of H<sub>2</sub>SO<sub>4</sub>-GICs. *J. Phys. Chem. Solids* **1996**, *57*, 889–892.
- (4) Mousavi Shaegh, S. A.; Nguyen, N. T.; Mousavi Ehteshami, S. M.; Chan, S. H. A membraneless hydrogen peroxide fuel cell using Prussian Blue as cathode material. *Energy Environ. Sci.* **2012**, *5*, 8225–8228.
- (5) Cao, D.; Gao, Y.; Wang, G.; Miao, R.; Liu, Y. A direct NaBH<sub>4</sub>-H<sub>2</sub>O<sub>2</sub> fuel cell using Ni foam supported Au nanoparticles as electrodes. *Int. J. Hydrogen Energy* **2010**, *35*, 807–813.
- (6) Wang, J. T.; Savinell, R. F.; Wainright, J.; Litt, M.; Yu, H. A H<sub>2</sub>/O<sub>2</sub> fuel cell using acid doped polybenzimidazole as polymer electrolyte. *Electrochim. Acta* **1996**, *41*, 193–197.
- (7) Park, S. Y.; et al. CaSnO<sub>3</sub>: An Electrocatalyst for Two-Electron Water Oxidation Reaction to Form H<sub>2</sub>O<sub>2</sub>. ACS Energy Lett. **2019**, 4, 352–357
- (8) Kelly, S. R.; et al. ZnO As an Active and Selective Catalyst for Electrochemical Water Oxidation to Hydrogen Peroxide. *ACS Catal.* **2019**, *9*, 4593–4599.
- (9) Fuku, K.; Sayama, K. Efficient oxidative hydrogen peroxide production and accumulation in photoelectrochemical water splitting using a tungsten trioxide/bismuth vanadate photoanode. *Chem. Commun.* **2016**, *52*, 5406–5409.
- (10) Xia, C.; et al. Confined local oxygen gas promotes electrochemical water oxidation to hydrogen peroxide. *Nat. Catal.* **2020**, *3*, 125–134.
- (11) Fuku, K.; Miyase, Y.; Miseki, Y.; Gunji, T.; Sayama, K. Enhanced Oxidative Hydrogen Peroxide Production on Conducting Glass Anodes Modified with Metal Oxides. *Chemistry Select* **2016**, *1*, 5721–5726.
- (12) Baek, J. H.; et al. Selective and Efficient Gd-Doped BiVO 4 Photoanode for Two-Electron Water Oxidation to  $H_2O_2$ . ACS Energy Lett. 2019, 4, 720–728.
- (13) Gill, T. M.; Zheng, X. Comparing Methods for Quantifying Electrochemically Accumulated  $H_2O_2$ . Chem. Mater. **2020**, 32, 6285–6294
- (14) Mavrikis, S.; Perry, S. C.; Leung, P. K.; Wang, L.; Ponce De León, C. Recent Advances in Electrochemical Water Oxidation to

- Produce Hydrogen Peroxide: A Mechanistic Perspective. ACS Sustainable Chem. Eng. 2021, 9, 76-91.
- (15) Shi, X.; Zhang, Y.; Siahrostami, S.; Kim, J. K.; Zheng, X. Light-driven BiVO<sub>4</sub>-C Fuel Cell with Simultaneous Production of H<sub>2</sub>O<sub>2</sub>. *Adv. Energy Mater.* **2018**, *8*, 1801158.
- (16) Miseki, Y.; Sayama, K. Photocatalytic Water Splitting for Solar Hydrogen Production Using the Carbonate Effect and the Z-Scheme Reaction. *Adv. Energy Mater.* **2019**, *9*, 1801294.
- (17) Liu, J.; Zou, Y.; Jin, B.; Zhang, K.; Park, J. H. Hydrogen Peroxide Production from Solar Water Oxidation. *ACS Energy Lett.* **2019**, *4*, 3018–3027.
- (18) Shi, X.; et al. Understanding activity trends in electrochemical water oxidation to form hydrogen peroxide. *Nat. Commun.* **2017**, *8*, 701.
- (19) Bard, A. J.; Jordan, J.; Parsons, R. Standard Potentials in Aqueous Solution; Marcel Dekker: New York, 1985.
- (20) De Laat, J.; Le, T. G. Effects of chloride ions on the iron(III)-catalyzed decomposition of hydrogen peroxide and on the efficiency of the Fenton-like oxidation process. *Appl. Catal., B* **2006**, *66*, 137–146.
- (21) Li, L.; Hu, Z.; Yu, J. C. On-Demand Synthesis of H<sub>2</sub>O<sub>2</sub> by Water Oxidation for Sustainable Resource Production and Organic Pollutant Degradation. *Angew. Chem., Int. Ed.* **2020**, *59* (46), 20538–20544.
- (22) Hall, S. B.; Khudaish, E. A.; Hart, A. L. Electrochemical Oxidation of Hydrogen Peroxide at Platinum Electrodes. Part 1. An Adsorption-Controlled Mechanism. *Electrochim. Acta* **1998**, 43 (5–6), 579–588.
- (23) Zhou, R.; Zheng, Y.; Jaroniec, M.; Qiao, S. Z. Determination of the Electron Transfer Number for the Oxygen Reduction Reaction: From Theory to Experiment. *ACS Catal.* **2016**, *6*, 4720–4728.
- (24) Xia, C.; Kim, J. Y.; Wang, H. Recommended practice to report selectivity in electrochemical synthesis of  $H_2O_2$ . *Nat. Catal.* **2020**, 3, 605–607.
- (25) Zhang, J.; Oloman, C. W. Electro-oxidation of carbonate in aqueous solution on a platinum rotating ring disk electrode. *J. Appl. Electrochem.* **2005**, *35*, 945–953.
- (26) Zhang, K.; Park, J. H.; Liu, J.; Wang, L.; Jin, B.; Yang, X.; Zhang, S. Near-Complete Suppression of Oxygen Evolution for Photoelectrochemical H<sub>2</sub>O Oxidative H<sub>2</sub>O<sub>2</sub> Synthesis. *J. Am. Chem. Soc.* **2020**, *142* (19), 8641–8648.
- (27) Richardson, D. E.; Yao, H.; Frank, K. M.; Bennett, D. A. Equilibria, kinetics, and mechanism in the bicarbonate activation of hydrogen peroxide: Oxidation of sulfides by peroxymonocarbonate. *J. Am. Chem. Soc.* **2000**, *122*, 1729–1739.
- (28) Patra, S. G.; Mizrahi, A.; Meyerstein, D. The Role of Carbonate in Catalytic Oxidations. Acc. Chem. Res. 2020, 53 (10), 2189–2200.
- (29) Lam, R. K.; et al. Reversed interfacial fractionation of carbonate and bicarbonate evidenced by x-ray photoemission spectroscopy. *J. Chem. Phys.* **2017**, *146*, 094703.
- (30) Zhao, K.; Wang, L.; Calizzi, M.; Moioli, E.; Züttel, A. In Situ Control of the Adsorption Species in CO<sub>2</sub> Hydrogenation: Determination of Intermediates and Byproducts. *J. Phys. Chem. C* **2018**, *122*, 20888–20893.
- (31) Jones, D. P.; Griffith, W. P. Alkali-metal peroxocarbonates,  $M_2[CO_3] \cdot nH_2O_2$ ,  $M_2[C_2O_6]$ ,  $M[HCO_4] \cdot nH_2O$ , and  $Li_2[CO_4] \cdot H_2O$ . J. Chem. Soc., Dalton Trans. **1980**, 0, 2526–2532.
- (32) Martínez-Hincapié, R.; Berná, A.; Rodes, A.; Climent, V.; Feliu, J. M. Surface Acid-Base Properties of Anion-Adsorbed Species at Pt(111) Electrode Surfaces in Contact with CO2-Containing Perchloric Acid Solutions. *J. Phys. Chem. C* **2016**, *120* (29), 16191–16199.
- (33) Wang, L.; Lu, Y.; Han, N.; Dong, C.; Lin, C.; Lu, S.; Min, Y.; Zhang, K. Suppressing Water Dissociation via Control of Intrinsic Oxygen Defects for Awakening Solar H<sub>2</sub>O-to-H<sub>2</sub>O<sub>2</sub> Generation. *Small* **2021**, *17* (13), 2100400.
- (34) Elgrishi, N.; et al. A Practical Beginner's Guide to Cyclic Voltammetry. J. Chem. Educ. 2018, 95, 197–206.

- (35) Bakhmutova-Albert, E. V.; Yao, H.; Denevan, D. E.; Richardson, D. E. Kinetics and mechanism of peroxymonocarbonate formation. *Inorg. Chem.* **2010**, *49*, 11287–11296.
- (36) Cristino, V.; et al. Efficient solar water oxidation using photovoltaic devices functionalized with earth-abundant oxygen evolving catalysts. *Phys. Chem. Chem. Phys.* **2013**, *15*, 13083–13092.
- (37) Kuttassery, F.; Sebastian, A.; Mathew, S.; Tachibana, H.; Inoue, H. Promotive Effect of Bicarbonate Ion on Two-Electron Water Oxidation to Form H<sub>2</sub>O<sub>2</sub> Catalyzed by Aluminum Porphyrins. *ChemSusChem* **2019**, 12 (9), 1939–1948.
- (38) Mavrikis, S.; Goltz, M.; Perry, S. C.; Bogdan, F.; Leung, P. K.; Rosiwal, S.; Wang, L.; Ponce de León, C. Effective Hydrogen Peroxide Production from Electrochemical Water Oxidation. *ACS Energy Lett.* **2021**, *6*, 2369–2377.